HHS Public Access

Author manuscript

J Orthop Res. Author manuscript; available in PMC 2023 July 01.

Published in final edited form as:

J Orthop Res. 2022 July ; 40(7): 1632–1644. doi:10.1002/jor.25187.

Compositional evaluation of lesion and parent bone in patients with juvenile osteochondritis dissecans of the knee using T_2* mapping

Štefan Zbýň[1,2],

Cassiano Santiago[1],

Casey P. Johnson[1,3],

Kai D. Ludwig[1,2],

Lin Zhang[4],

Shelly Marette[2],

Marc A. Tompkins[5,6,7],

Bradley J. Nelson[5,6],

Takashi Takahashi[2],

Gregory J. Metzger[1],

Cathy S. Carlson[3],

Jutta M. Ellermann[1,2]

[1]Center for Magnetic Resonance Research, University of Minnesota, Minneapolis, Minnesota, USA

[2]Department of Radiology, University of Minnesota, Minneapolis, Minnesota, USA

[3]Department of Veterinary Clinical Sciences, University of Minnesota, St. Paul, Minnesota, USA

[4]Division of Biostatistics, School of Public Health, University of Minnesota, Minneapolis, Minnesota, USA

[5]Department of Orthopedic Surgery, University of Minnesota, Minneapolis, Minnesota, USA

[6]TRIA Orthopedic Center, Minneapolis, Minnesota, USA

[7]Gillette Children's Specialty Healthcare, St. Paul, Minnesota, USA

Abstract

Juvenile osteochondritis dissecans (JOCD) lesions contain cartilaginous, fibrous and osseous tissues which are difficult to distinguish with clinical, morphological magnetic resonance imaging (MRI). Quantitative T_2* mapping has earlier been used to evaluate microstructure and composition of all aforementioned tissues as well as bone mineral density. However, the ability of T_2* mapping to detect changes in tissue composition between different JOCD lesion regions, different disease stages, and between stable and unstable lesions has not been demonstrated. This

Correspondence Štefan Zbýň, Center for Magnetic Resonance Research, Department of Radiology, University of Minnesota, 2021 6th St SE, Minneapolis, MN 55455, USA. szbyn@umn.edu.

study analyzed morphological and T_2* MRI data from 25 patients (median age, 12.1 years) with 34 JOCD-affected and 13 healthy knees. Each lesion was assigned a stage reflecting the natural history of JOCD, with stages I and IV representing early and healed lesion, respectively. T_2* values were evaluated within the progeny lesion, interface and parent bone of each lesion and in the control bone region. T_2* was negatively correlated with JOCD stage in progeny lesion ($\rho = -0.871$; $p < 0.001$) and interface regions ($\rho = -0.649$; $p < 0.001$). Stage IV progeny showed significantly lower T_2* than control bone ($p = 0.028$). T_2* was significantly lower in parent bone than in control bone of patients with stable lesions ($p = 0.009$), but not in patients with unstable lesions ($p = 0.14$). Clinical significance: T_2* mapping enables differentiation between different stages of JOCD and quantitative measurement of the ossification degree in progeny lesion and interface. The observed T_2* decrease in healed and stable lesions may indicate increased bone density as a result of the active repair process. T_2* mapping provides quantitative information about JOCD lesion composition.

Keywords

compositional magnetic resonance imaging; juvenile osteochondritis dissecans; knee joint; T_2*; trabecular bone

1 | INTRODUCTION

Juvenile osteochondritis dissecans (JOCD) is a developmental joint disorder commonly manifested as an osteochondral lesion of the distal femoral condyle,[1–4] affecting 6–10 of 100,000 children aged 6–19 years.[5,6] Comparative studies suggest a similar pathogenesis in humans and animals with the disease onset related to ischemic necrosis of epiphyseal (subarticular) cartilage and subsequent failure of endochondral ossification.[7–9] Over time, the necrotic epiphyseal cartilage (aka “progeny lesion”) may either heal by becoming a part of subchondral “parent” bone or progress to clefting and eventual creation of a bony fragment.[1–3] Although the lesion ossification has an important role in the pathogenesis,[2] the natural history of JOCD is still not entirely understood.[10]

The majority of previous magnetic resonance imaging (MRI) studies focused on the morphological assessment of JOCD lesions with particular attention to describe status of the underlying articular cartage and the main three JOCD regions: the progeny lesion, the parent bone and the interface between them.[1–3,10,11] Clinical, morphological MRI can differentiate between stable and unstable lesions, and help guide JOCD management.[4] The interface between progeny lesions and parent bone plays an important role in the evaluation of lesion stability with the presence of multiple cysts or one large cyst suggesting unstable JOCD lesion.[4] Unstable, symptomatic lesions are treated surgically,[12] while conservative treatment for 6–12 months is recommended for stable lesions.[13,14] Unfortunately, conservative treatment of stable lesions fails in up to 50% of patients.[13,15–17] Although predictors such as age, lesion size, and presence of cystic changes in lesion seem to be associated with treatment success,[16] it is still not possible to reliably predict which lesions will heal and which not. Therefore there is a demand for new, noninvasive MRI biomarkers that are able to predict which lesions will heal and which will become unstable before the morphological

signs of instability are visible on clinical, morphological MR images. Noninvasive MRI biomarkers enabling reliable prediction of treatment outcome for conservatively treated stable JOCD lesions (i.e., knee immobilization, limited weight-bearing, activity restriction) may significantly shorten the recommended 6–12 months of nonoperative treatment[13,14] for lesions that are unlikely to benefit from such therapy, and thus improve clinical management of JOCD patients.

Clinical, morphological MRI relies on spin echo sequences with long (≥20 ms) echo times (TE) that cannot unambiguously distinguish between the cartilaginous, fibrous and osseous tissues found within JOCD lesions in previous histological studies.[18–20] The novel concept of short TE, morphological MRI with CT-like contrast was recently introduced to improve the visualization of osseous tissues in JOCD lesions.[2] Additionally, these MRI techniques were used for staging of JOCD lesions based on depiction of osseous tissue in the progeny lesion and presence of osseous bridging to the interface.[2] Unfortunately, clinical MRI and short TE, morphological MRI with CT-like contrast are not able to provide information about the structural composition of osseous tissue in JOCD lesions. MRI techniques able to evaluate structure and composition of tissues within JOCD lesions could, therefore, provide new insights into the process of lesion healing.

Here, we propose T_2* mapping for the compositional evaluation of osseous and other tissues within JOCD lesions. T_2* is the transverse relaxation time constant that characterizes how fast the MR signal (i.e., the transverse component of magnetization) decays in the tissue in the presence of local static magnetic field inhomogeneities. T_2* values reflect the interactions between the magnetic moments of water and the surrounding macromolecules in the given tissue and therefore provides indirect measurement of tissue microstructure and composition.[21,22] Quantitative T_2* mapping has been successfully used to evaluate microstructure and composition of the articular cartilage,[23,24] fibrocartilage,[25] and trabecular bone.[26–29] Previously reported T_2* values in cartilage (~23 ms) [23,24] and fibrocartilage (~19 ms) [25] are much higher compared to T_2* in trabecular bone (~4 ms),[30–32] T_2* mapping should therefore allow differentiation between cartilaginous and osseous regions within JOCD lesions. Furthermore, magnetic susceptibility differences between bone trabeculae and marrow impose static field inhomogeneities and causes shortening of T_2* values. T_2* values in the bone marrow thus provide indirect information about the structure and density of surrounding trabecular architecture.[33–35] This unique feature of T_2* mapping was used in bone marrow studies that showed significantly longer T_2* in patients with osteoporosis compared to control subjects and demonstrated negative correlation between T_2* values and bone mineral density in femur, calcaneus and lumbar spine.[26–29] Noninvasive T_2* mapping may therefore provide a useful continuous metric for differentiation and quantitative evaluation of cartilaginous and osseous tissue components as well as indirect assessment of trabecular bone quality in JOCD lesions.

Considering the difference in T_2* values between articular cartilage [23,24] and trabecular bone [26–29] reported in previous studies, the goal of the present study was to determine if T_2* mapping allows noninvasive, quantitative assessment of all lesion tissues (i.e., cartilaginous and osseous) and evaluation of their structure and composition in JOCD patients. Therefore, we retrospectively evaluated participants with JOCD lesions in distal femoral condyle

to assess ability of quantitative T_2* mapping to detect differences in tissue composition between: (i) different regions within JOCD lesions, (ii) different JOCD stages, and (iii) between stable and unstable JOCD lesions.

2 | METHODS

2.1 | Study population

This retrospective observational cohort study (level of evidence: 3) adhered to Health Insurance Portability and Accountability Act and was approved by the institutional review board that waived the need for informed consent. Between December 2015 and March 2020, a total of 37 young patients with initial diagnosis of JOCD underwent 3T MRI including T_2* mapping at our institution. From the cohort of 37 patients, two patients were excluded because their lesions were diagnosed as ossification variants.[36] Four patients were excluded because of the absence of an open growth plate in the distal femur. Six patients were excluded due to the prior surgery in the evaluated knee. Finally, 25 patients with JOCD of the knee were included into our evaluations. Exclusion criteria and the corresponding numbers of excluded participants are summarized in Figure 1. None of patients showed signs of knee arthritis, malignancy, or severe MRI artifacts. Due to the relatively high prevalence of bilateral JOCD lesions, both knees were imaged. Inclusion criteria for healthy, control knees were absence of clinical symptoms in the knee (e.g. pain, clicking, locking), no JOCD lesion, and no abnormal MRI findings (e.g. bone marrow lesions, cartilage, or meniscus abnormalities).

2.2 | MRI protocol

All images were acquired on a whole-body 3T MRI system (Prisma Fit; Siemens Healthcare) using a single-channel transmit, 15-channel receive phased-array knee coil (Quality Electrodynamics). The protocol included morphological T_2-weighted, T_1-weighted, and proton density-weighted turbo-spin echo sequences with and without fat suppression. For the evaluation of T_2* relaxation times, a multislice multiecho gradient recalled echo (GRE) sequence was acquired with following parameters: repetition time = 1150 ms; six TEs = 2.6, 5.6, 8.5, 11.5, 14.5 and 17.4 ms; in plane resolution = 0.43 × 0.43 mm^2; slice thickness = 2.0 mm; acquisition time of about 6 min (depending on the number of acquired slices). The TEs were selected as a compromise between the signal-to-noise ratio in the trabecular bone marrow, amount of data points for fitting of short T_2* in bone marrow, longest TE close to expected T_2* of cartilage and the total acquisition time below 7 min. All six TEs were acquired with a single multiecho GRE sequence. The short echo images of the T_2* mapping sequence are routinely clinically reviewed by the radiologists at our institution for the evaluation of osseous components within lesion and assignment of JOCD stage[2] described in the following section. Acquisition parameters of all MRI sequences are detailed in Table 1.

2.3 | Lesion stability and staging

Two musculoskeletal radiologists (S.M. and J.M.E., both with 15 years of experience) independently evaluated the lesion stability on clinical, morphological MR images by using the morphologic features of instability as previously described by Kijowski et al.[4] An

unstable JOCD lesion was defined as the presence of articular cartilage fracture and/or the presence of four secondary signs: a rim of fluid signal intensity, a second outer rim of low T_2 signal intensity, multiple breaks in the subchondral plate, and a large or multiple cyst(s).[4] After independent evaluations of lesion stability, all lesions that were evaluated differently were reviewed and the two radiologists came to a consensus in each JOCD lesion.

Two fellowship-trained musculoskeletal radiologists (S.M. and J.M.E.) without prior access to the patients' clinical history and T_2* maps independently assigned each lesion to one JOCD stage according to previously described staging system [2] based on qualitative depiction of osseous tissues in the progeny lesion and its interface to parent bone on morphological, short TE GRE images with CT-like contrast. This system divides JOCD lesions into 5 stages: (I) epiphyseal cartilage lesion with delay in endochondral ossification (Figure 2A); (II) peripheral ossification of the progeny (Figure 2B); (III) partial ossification of the progeny with partial osseous bridging (Figure 2C); (IV) completely ossified progeny with complete osseous bridging—healed or almost healed lesion (Figure 2D); or (V) not-healed detached lesion. Lesions that showed evidence of two different stages were assigned a stage representing the majority of lesion volume. After independent staging, the two radiologists performed a review of all lesions they staged differently and came to a consensus in each case.

2.4 | Segmentations and quantitative evaluations

Manual 3D segmentations were performed on the T_2*-weighted images with the shortest TE using ITK-SNAP,[37] with readers having access to morphological MRI (Figure 3A,B) but not to the T_2* maps. In JOCD knees, four regions, including three regions within JOCD lesion complex and a control bone region, were segmented as depicted in Figure 3C. The progeny lesion, the parent bone and the interface between them are the three distinct JOCD regions, each having specific morphologic features and a unique role during the disease progression.[1–3,10,11] The progeny lesion region was segmented to encompass the entire progeny area. The interface region was selected between progeny lesion and adjacent trabecular bone. The parent bone region was selected to encompass the sclerotic bone adjacent to the interface region. The control bone region was segmented within trabecular bone of the contralateral, lesion-free femoral condyle. In healthy, JOCD-free knees, only the control bone region was segmented matching the control bone region in JOCD knee of the same patient. To provide one representative T_2* value for healthy control bone that could be compared to T_2* values from all three regions within JOCD lesion (i.e. progeny lesion, interface, parent bone) we attempted to match the size of the control bone region to the combined size of progeny lesion, interface and parent bone regions. All regions were segmented by a radiology resident (C.S.) in consensus with an expert musculoskeletal radiologist (J.M.E.). For the evaluation of interobserver reproducibility, a musculoskeletal MRI physicist (Š.Z., 11 years of experience) independently segmented the regions in 10 randomly selected JOCD knees.

All T_2* maps were calculated on a pixel-wise basis by fitting the MR signal to the model of signal decay using a two-parametric nonlinear least-square fitting with the Levenberg-

Marquardt algorithm in Matlab (R2017b; MathWorks) (Figure 3E). Following exponential model was fitted to multiecho data with all TEs contributing equally

$$S = M_0 \exp\left(-TE/T_2^*\right),$$

where TE is the echo time, S is measured MR signal at a given TE, and the parameters M_0 and T_2* are estimated magnetization in equilibrium and T_2* relaxation time, respectively (Figure 4D–F). The corresponding coefficient of determination (R^2) maps were calculated to evaluate the percentage of variation explained by the fitting model (Figure 3F). Median T_2* and R^2 values were calculated from the progeny lesion, interface, parent bone and control bone 3D regions. Additionally, region volumes were calculated by multiplying a region's pixel count with the pixel volume of the T_2*-weighted images.

2.5 | Statistical methods

Agreement between the two radiologists evaluating stability and stage of JOCD lesions was calculated with the Cohen's κ. The mixed effects regression models, with age, sex and lesion volume as covariates and adjustment for within-subject variability, were followed by Tukey's posthoc tests to compare T_2* values between the segmented regions, the JOCD stages (I–IV), the healthy and JOCD knees, and the stable and unstable lesions. The same tests were used to compare the lesion volume between the JOCD stages. p values were adjusted for multiple pair-wise comparisons. Age and lesion volume differences between the stable and unstable lesions were evaluated with independent samples t tests. The inter-reader reproducibility of T_2* evaluations was assessed by the Pearson's correlation coefficients and the coefficients of variance. Spearman rank correlation coefficients (ρ) were calculated to evaluate the correlations of T_2* and region volume with JOCD stage and patient's age. Statistical significance was indicated by a $p < 0.05$. All evaluated data were examined for normal distribution using Box plots and Q-Q plots. Region volumes were normalized by calculating the cube root of volume to ensure the normal distribution of data before further statistical evaluations. Statistical analyses were calculated in R (3.5.1; Foundation for Statistical Computing).

3 | RESULTS

3.1 | Patient cohort

A total of 25 patients (16 boys [median age, 13.2 years; interquartile range [IQR], 11.7–14.9 years], 9 girls [median age, 11.6 years; IQR, 9.8–12.7 years]) met all inclusion criteria and were enrolled in this study (Table 2). This cohort presented with 34 JOCD-affected knees and 13 lesion-free knees. From 22 patients with bilateral MRI, nine (41%) had JOCD lesions in both knees. All 34 lesions were divided into four subgroups according to the JOCD staging system.[2] The staging of lesions by the two independent radiologists resulted in high inter-rater agreement with a Cohen's κ of 0.838 (95% confidence interval [CI] = 0.689, 0.988) and agreement in 30 out of 34 (88%) lesions.

Eleven of the 34 JOCD lesions were evaluated as unstable using the morphological MRI criteria of instability.[4] The evaluation of lesion stability by the two independent radiologists

resulted in substantial inter-reader agreement with a Cohen's κ of 0.656 (95% CI = 0.381, 0.931) and agreement in 29 out of 34 (85%) JOCD lesions. All unstable lesions were surgically treated after the MRI (median interval, 47 days; IQR, 28–100 days). Example morphological MR images and a T_2* map of unstable JOCD lesion are illustrated in the Figure 4. From 23 stable lesions, 11 lesions were selected to match for JOCD stage and other patient characteristics of unstable lesion group (Table 2). No statistically significant difference in age was observed between stable and unstable groups ($p = 0.07$). All patients from stable lesions group became asymptomatic during conservative treatment (shortest follow-up, 12 months) and three JOCD lesions were confirmed by imaging to heal.

3.2 | Lesion regions

The comparisons between evaluated regions found significantly higher T_2* values in the progeny lesion than in the parent and control bone regions at JOCD stages I–III (all $p \leq 0.025$) (Table 3). At stage IV, progeny lesion T_2* was significantly lower than control bone T_2* ($p = 0.028$), but not than parent bone T_2* ($p = 0.45$). This difference is demonstrated on T_2* map in the Figure 5. Additionally, interface T_2* was significantly higher than parent bone T_2* at stages II and III, and control bone T_2* at stage II (all $p \leq 0.006$). Although differences were not statistically significant, T_2* was lower in parent bone than in control bone at all JOCD stages (all $p \geq 0.17$). Furthermore, control bone T_2* was not significantly different between the control knees (median, 5.0 ms; IQR, 4.6–5.4 ms) and the JOCD knees (median, 4.8 ms; IQR, 4.4–5.3 ms) of the same patients ($p = 0.06$). Median R^2 values in all regions were higher than 0.91 indicating reliable T_2* fitting.

3.3 | JOCD stages

The comparisons between different JOCD stages showed significantly higher T_2* in progeny lesion at stages I and II than at stages III and IV (all $p \leq 0.011$) (Table 4). The interface showed significantly lower T_2* at stage IV compared to stages I–III (all $p \leq 0.046$). No significant differences between different JOCD stages were found in parent bone T_2*, control bone T_2*, or volume of progeny lesion (all $p \geq 0.12$).

The Spearman rank correlations showed a significant negative association between the JOCD stage and T_2* in the progeny lesion ($\rho = -0.871$; 95% CI = −0.936, −0.732; $p < 0.001$) and in the interface ($\rho = -0.649$; 95% CI = −0.834, −0.364; $p < 0.001$) (Figure 6). While no significant correlation was observed between the age and T_2* in all regions, the age was significantly correlated with the volume of progeny lesion ($\rho = 0.534$; 95% CI = 0.123, 0.753; $p = 0.001$), interface ($\rho = 0.477$; 95% CI = 0.165, 0.704; $p = 0.004$), and parent bone ($\rho = 0.415$; 95% CI = 0.106, 0.681; $p = 0.014$). No correlation was found between the age and the JOCD stage ($\rho = 0.081$; 95% CI = −0.331, 0.477; $p = 0.65$) (Figure 6). All evaluated Spearman rank correlations are listed in the Table 5.

3.4 | Stable versus unstable JOCD lesions

Although T_2* values in the interface and parent bone were higher in unstable than in stable JOCD lesions, no significant differences were observed in any of evaluated regions between unstable and stable lesions (all $p \geq 0.27$) (Figure 7). We found significantly lower T_2* in parent bone than in control bone of patients with stable lesions ($p = 0.009$). However, no

statistically significant difference was observed between the parent bone and control bone of patients with unstable lesions ($p = 0.14$) (Figure 7). Our results showed that the volume of progeny lesion was significantly higher in unstable than in stable JOCD lesions ($p = 0.002$) (Table 6).

3.5 | Inter-reader repeatability

High inter-reader repeatability was found for T_2* evaluations. The Pearson's correlation coefficients between the two readers were 0.997 in progeny lesion (95% CI = 0.987, 0.999; $p < 0.001$), 0.991 in interface (95% CI = 0.963, 0.998; $p < 0.001$), 0.885 in parent bone (95% CI = 0.576, 0.973; $p < 0.001$), and 0.983 in control bone (95% CI = 0.927, 0.996; $p < 0.001$). The mean coefficients of variation between the two readers were 5.7% in progeny lesion, 6.9% in interface, 4.7% in parent bone, and 2.0% in control bone.

4 | DISCUSSION

This is the first study to investigate the ability of T_2* mapping to detect differences in tissue composition between different lesion regions, different disease stages, as well as between stable and unstable lesions of JOCD patients. We demonstrated that T_2* mapping allows quantitative evaluation of osseous, fibrous, and cartilaginous tissues in JOCD lesions and can therefore measure the degree of ossification in progeny and interface, which are important factors in lesion healing but are difficult to evaluate with morphological MRI. Our findings suggest that T_2* mapping can detect increased bone density in progeny lesion and parent bone which may indicate an active process of lesion repair. This study demonstrates that the addition of T_2* mapping to the standard clinical MRI protocol provides the noninvasive imaging tool for quantitative tissue characterization, otherwise only attainable by histology. T_2* mapping is a promising method with a potential to improve clinical management of JOCD patients.

We found a progressively decreasing T_2* values with increasing JOCD stage in progeny lesion and interface which is due to the gradual ossification of lesion. The T_2* of progeny lesion at stage I was high and similar to previously reported T_2* of articular cartilage[23,24] and fibrocartilage,[25] while the progeny T_2* at stage IV was low and similar to the T_2* of trabecular bone.[30–32] These results emphasize the role of progressive ossification in lesion healing in the natural history of JOCD,[2,7–9,18] and confirm the previously proposed JOCD staging system based on qualitative evaluation of osseous tissues on short TE GRE images with CT-like contrast.[2] The T_2* mapping allows quantitative evaluation of all tissues present in JOCD lesions[18–20] while allowing the differentiation between osseous and fibrous tissues, which are difficult to distinguish on standard clinical, morphological MRI sequences with long (≥20 ms) TE. Quantitative measurement of the degree of tissue ossification using T_2* mapping may provide important insights into JOCD lesion healing.

Our results showed significantly lower T_2* in stage IV progeny lesion, signaling a different composition of osseous progeny compared to the healthy, control bone. Significantly lower T_2* values were also found in the parent bone of stable (stage II and III) lesions, but not in the parent bone of unstable (stages II and III) lesions when compared to control bone. All patients with unstable lesions received surgery while all patients with stable lesions

became asymptomatic (shortest follow-up of 12 months) and three lesions were confirmed by imaging to heal. Previous in vivo studies reported significant negative correlations of T_2* with bone density evaluated by dual energy X-ray absorptiometry in different skeletal locations including calcaneus, lumbar spine and femoral neck.[26–29] Lower T_2* values probably indicate increased bone density in progeny lesion and parent bone of patients with stable, healing JOCD lesions. This explanation is supported by histological studies that demonstrated increased bone formation, bone resorption and osteoid accumulation in stable JOCD lesions, which are typical characteristics of active tissue repair.[19,38–40] Correspondingly, the absence of significantly lower T_2* in parent bone of unstable lesions may suggest an absence of active healing processes. Our findings suggest that T_2* mapping can detect increased bone density in progeny lesion and parent bone which may indicate active lesion repair, however, future studies are necessary to confirm this relationship. If confirmed, T_2* mapping may provide a new, noninvasive biomarker of lesion repair and thus inform treatment decision in JOCD patients.

We observed almost perfect inter-rater agreement in lesion staging and substantial agreement in the evaluation of lesion instability between two independent radiologists. While the inter-reader agreement for staging of JOCD lesions was not previously evaluated, relatively low interrater reliability of lesion instability assessment was reported.[11,41] Additionally, high interobserver repeatability of T_2* evaluations was found in all evaluated regions. Furthermore, all regions showed median R^2 values higher than 0.91 indicating that at least 91% percent of the variation in T_2* data can be explained by the fitting model, thus suggesting reliable T_2* mapping in all evaluated tissues. These findings demonstrate that T_2* mapping is reproducible, reader independent method that can serve as an objective outcome measure for the quantitative assessment of JOCD lesions.

While factors such as age, symptoms and lesion location were very similar between the patient groups with stable and unstable JOCD lesions, we observed significantly larger volume of progeny lesion in patients with unstable than with stable lesions. In previous study, lesion width and patient age have been reported to be among the most significant factors for the prediction of lesion healing.[16] Additionally, in the present study, T_2* in the interface tended to be higher in unstable than in stable lesions which is likely due to the presence of fluid in the interface which was detected with clinical, morphological MRI in eight unstable lesions. All unstable lesions were found at stages II and III but not at stage I, which may suggest that the progeny lesion has to be at least partially ossified before the instability can develop. Although a positive association between the JOCD stage and age was reported previously,[2] we did not observe any significant correlation between these parameters in this study. This could be due to the absence of stage V lesions and the exclusion of patients with a closed femoral growth plate in the current study, or because of the small number of stage I ($n = 1$) and stage IV ($n = 2$) lesions in the previous report.[2] However, we found positive correlation between the age and the volume of progeny lesion, interface and parent bone, indicating that older patients tend to have larger JOCD lesions.

This study has several limitations. First, 34 JOCD lesions is a relatively small sample size. This is mainly due to single-center study design and the rarity of this disease. Second, groups of patients with different JOCD stage were not matched for age, sex or number of

subjects due to the retrospective nature of the study. However, no significant correlation was observed between the T_2* and patient's age in any region, including control bone. Third, lesion-free asymptomatic contralateral knees of JOCD patients without abnormalities on morphological MRI were used as controls. While the biomechanics of control knees might have been altered due to the symptoms in JOCD-affected knees, this approach enabled comparisons between the perfectly age- and sex-matched groups. Fourth, this study doesn't compare T_2* results to the gold-standard histopathological analysis or to the dual energy X-ray absorptiometry. This is due to retrospective nature of this study and the fact that these methods are not routinely used for the evaluation of pediatric JOCD patients. Finally, since TEs used in this study are neither in phase nor out of phase, a combination of water and fat MR signals was used in the present T_2* analyses of bone marrow. Possible differences in fat and water fractions between the patients might therefore have contributed to the T_2* differences observed in this study. Future studies using multiecho GRE sequence optimized for water-fat separation[22,31,42] are needed to evaluate possible changes in proton density fat fraction during the process of JOCD lesion healing.

In conclusion, T_2* mapping of JOCD lesions allows excellent inter-reader reproducibility, enables evaluation of osseous, fibrous, and cartilaginous tissues in JOCD lesions, and thus provides quantitative measurement of degree of ossification in progeny lesion and interface regions. Furthermore, T_2* results suggest different quality of osseous tissue in recently healed progeny lesions and in parent bone of stable lesions when compared to healthy trabecular bone in JOCD patients. T_2* is a potential imaging biomarker of lesion healing that may be useful in planning and monitoring nonsurgical treatment of JOCD patients. Future studies comparing T_2* results with histology or dual energy X-ray absorptiometry as well as longitudinal T_2* studies are warranted to further validate these promising results and to assess the potential of T_2* in lesion and parent bone as a predictor of JOCD healing.

ACKNOWLEDGMENTS

This study was supported by National Institutes of Health, including the National Institute of Arthritis and Musculoskeletal and Skin Diseases (R01 AR070020, K01 AR070894, T32 AR050938), and National Institute of Biomedical Imaging and Bioengineering (P41 EB027061). Authors have no financial or other conflicts to declare.

Funding information

National Institute of Biomedical Imaging and Bioengineering, Grant/Award Number: P41 EB027061; National Institute of Arthritis and Musculoskeletal and Skin Diseases, Grant/Award Numbers: K01 AR070894, R01 AR070020, T32 AR050938

REFERENCES

1. Laor T, Zbojniewicz AM, Eismann EA, Wall EJ. Juvenile osteochondritis dissecans: is it a growth disturbance of the secondary physis of the epiphysis? AJR Am J Roentgenol. 2012;199:1121–1128. [PubMed: 23096188]
2. Ellermann J, Johnson CP, Wang L, Macalena JA, Nelson BJ, LaPrade RF. Insights into the epiphyseal cartilage origin and subsequent osseous manifestation of juvenile osteochondritis dissecans with a modified clinical MR imaging protocol: a pilot study. Radiology. 2017;282:798–806. [PubMed: 27631413]
3. Gorbachova T, Melenevsky Y, Cohen M, Cerniglia BW. Osteochondral lesions of the knee: differentiating the most common entities at MRI. Radiographics. 2018;38:1478–1495. [PubMed: 30118392]

4. Kijowski R, Blankenbaker DG, Shinki K, Fine JP, Graf BK, De Smet AA. Juvenile versus adult osteochondritis dissecans of the knee: appropriate MR imaging criteria for instability. Radiology. 2008;248:571–578. [PubMed: 18552309]
5. Kessler JI, Nikizad H, Shea KG, Jacobs JC Jr, Bebchuk JD, Weiss JM. The demographics and epidemiology of osteochondritis dissecans of the knee in children and adolescents. Am J Sports Med. 2014;42:320–326. [PubMed: 24272456]
6. Pareek A, Sanders TL, Wu IT, Larson DR, Saris D, Krych AJ. Incidence of symptomatic osteochondritis dissecans lesions of the knee: a population-based study in Olmsted County. Osteoarthritis Cartilage. 2017;25:1663–1671. [PubMed: 28711583]
7. Olstad K, Ekman S, Carlson CS. An update on the pathogenesis of osteochondrosis. Vet Pathol. 2015;52:785–802. [PubMed: 26080832]
8. Tóth F, Tompkins MA, Shea KG, Ellermann JM, Carlson CS. Identification of areas of epiphyseal cartilage necrosis at predilection sites of juvenile osteochondritis dissecans in pediatric cadavers. J Bone Joint Surg Am. 2018;100:2132–2139. [PubMed: 30562294]
9. Ellermann JM, Ludwig KD, Nissi MJ, et al. Three-dimensional quantitative magnetic resonance imaging of epiphyseal cartilage vascularity using vessel image features: new insights into juvenile osteochondritis dissecans. JBJS Open Access. 2019;4:1–9.
10. Edmonds EW, Polousky J. A review of knowledge in osteochondritis dissecans: 123 years of minimal evolution from Konig to the ROCK study group. Clin Orthop Relat Res. 2013;471:1118–1126. [PubMed: 22362466]
11. Fabricant PD, Milewski MD, Kostyun RO, et al. Osteochondritis dissecans of the knee: an interrater reliability study of magnetic resonance imaging characteristics. Am J Sports Med. 2020;48:2221–2229. [PubMed: 32584594]
12. Hevesi M, Sanders TL, Pareek A, et al. Osteochondritis dissecans in the knee of skeletally immature patients: rates of persistent pain, osteoarthritis, and arthroplasty at mean 14-years' follow-up. Cartilage. 2020;11:291–299. [PubMed: 29998745]
13. Robertson W, Kelly BT, Green DW. Osteochondritis dissecans of the knee in children. Curr Opin Pediatr. 2003;15:38–44. [PubMed: 12544270]
14. Flynn JM, Kocher MS, Ganley TJ. Osteochondritis dissecans of the knee. J Pediatr Orthop. 2004;24:434–443. [PubMed: 15205627]
15. Cahill BR, Phillips MR, Navarro R. The results of conservative management of juvenile osteochondritis dissecans using joint scintigraphy. A prospective study. Am J Sports Med. 1989;17:601–605. [PubMed: 2610273]
16. Krause M, Hapfelmeier A, Möller M, Amling M, Bohndorf K, Meenen NM. Healing predictors of stable juvenile osteochondritis dissecans knee lesions after 6 and 12 months of nonoperative treatment. Am J Sports Med. 2013;41:2384–2391. [PubMed: 23876519]
17. Hughes JA, Cook JV, Churchill MA, Warren ME. Juvenile osteochondritis dissecans: a 5-year review of the natural history using clinical and MRI evaluation. Pediatr Radiol. 2003;33:410–417. [PubMed: 12684712]
18. Uozumi H, Sugita T, Aizawa T, Takahashi A, Ohnuma M, Itoi E. Histologic findings and possible causes of osteochondritis dissecans of the knee. Am J Sports Med. 2009;37:2003–2008. [PubMed: 19737988]
19. Krause M, Lehmann D, Amling M, et al. Intact bone vitality and increased accumulation of nonmineralized bone matrix in biopsy specimens of juvenile osteochondritis dissecans: a histological analysis. Am J Sports Med. 2015;43:1337–1347. [PubMed: 25759459]
20. Zbojniewicz AM, Stringer KF, Laor T, Wall EJ. Juvenile osteochondritis dissecans: correlation between histopathology and MRI. AJR Am J Roentgenol. 2015;205:W114–W123. [PubMed: 26102409]
21. Burstein D, Gray M. New MRI techniques for imaging cartilage. J Bone Joint Surg Am. 2003;85(A Suppl 2):70–77. [PubMed: 12721347]
22. Karampinos DC, Ruschke S, Dieckmeyer M, et al. Quantitative MRI and spectroscopy of bone marrow. J Magn Reson Imaging. 2018;47:332–353. [PubMed: 28570033]

23. Welsch GH, Apprich S, Zbyn S, et al. Biochemical (T2, T2* and magnetisation transfer ratio) MRI of knee cartilage: feasibility at ultra-high field (7T) compared with high field (3T) strength. Eur Radiol. 2011;21: 1136–1143. [PubMed: 21153551]
24. Ludwig KD, Johnson CP, Zbýň Š, et al. MRI evaluation of articular cartilage in patients with juvenile osteochondritis dissecans (JOCD) using T2* mapping at 3T. Osteoarthritis Cartilage. 2020;28:1235–1244. [PubMed: 32278071]
25. Mamisch TC, Hughes T, Mosher TJ, et al. T2 star relaxation times for assessment of articular cartilage at 3 T: a feasibility study. Skeletal Radiol. 2012;41:287–292. [PubMed: 21499976]
26. Link TM, Majumdar S, Augat P, et al. Proximal femur: assessment for osteoporosis with T2* decay characteristics at MR imaging. Radiology. 1998;209:531–536. [PubMed: 9807585]
27. Kang C, Paley M, Ordidge R, Speller R. In vivo MRI measurements of bone quality in the calcaneus: a comparison with DXA and ultrasound. Osteoporos Int. 1999;9:65–74. [PubMed: 10367031]
28. Maris TG, Damilakis J, Sideri L, et al. Assessment of the skeletal status by MR relaxometry techniques of the lumbar spine: comparison with dual X-ray absorptiometry. Eur J Radiol. 2004;50:245–256. [PubMed: 15145484]
29. Wu HZ, Zhang XF, Han SM, et al. Correlation of bone mineral density with MRI T2* values in quantitative analysis of lumbar osteoporosis. Arch Osteoporos. 2020;15:18. [PubMed: 32088768]
30. Du J, Hermida JC, Diaz E, et al. Assessment of cortical bone with clinical and ultrashort echo time sequences. Magn Reson Med. 2013;70:697–704. [PubMed: 23001864]
31. Karampinos DC, Melkus G, Baum T, Bauer JS, Rummeny EJ, Krug R. Bone marrow fat quantification in the presence of trabecular bone: initial comparison between water-fat imaging and single-voxel MRS. Magn Reson Med. 2014;71:1158–1165. [PubMed: 23657998]
32. Jerban S, Lu X, Dorthe EW, et al. Correlations of cortical bone microstructural and mechanical properties with water proton fractions obtained from ultrashort echo time (UTE) MRI tricomponent T_2* model. NMR Biomed. 2020;33:e4233. [PubMed: 31820518]
33. Davis CA, Genant HK, Dunham JS. The effects of bone on proton NMR relaxation times of surrounding liquids. Invest Radiol. 1986;21:472–477. [PubMed: 3721804]
34. Sebag GH, Moore SG. Effect of trabecular bone on the appearance of marrow in gradient-echo imaging of the appendicular skeleton. Radiology. 1990;174:855–859. [PubMed: 2305069]
35. Majumdar S, Thomasson D, Shimakawa A, Genant HK. Quantitation of the susceptibility difference between trabecular bone and bone marrow: experimental studies. Magn Reson Med. 1991;22:111–127. [PubMed: 1798386]
36. Jans L, Jaremko J, Ditchfield M, et al. Ossification variants of the femoral condyles are not associated with osteochondritis dissecans. Eur J Radiol. 2012;81:3384–3389. [PubMed: 22297186]
37. Yushkevich PA, Piven J, Hazlett HC, et al. User-guided 3D active contour segmentation of anatomical structures: significantly improved efficiency and reliability. Neuroimage. 2006;31: 1116–1128. [PubMed: 16545965]
38. Chiroff RT, Cooke CP 3rd. Osteochondritis dissecans: a histologic and microradiographic analysis of surgically excised lesions. J Trauma. 1975;15:689–696. [PubMed: 807740]
39. Koch S, Kampen WU, Laprell H. Cartilage and bone morphology in osteochondritis dissecans. Knee Surg Sports Traumatol Arthrosc. 1997;5:42–45. [PubMed: 9127853]
40. Yonetani Y, Nakamura N, Natsuume T, Shiozaki Y, Tanaka Y, Horibe S. Histological evaluation of juvenile osteochondritis dissecans of the knee: a case series. Knee Surg Sports Traumatol Arthrosc. 2010;18:723–730. [PubMed: 19760400]
41. Haeri Hendy S, de Sa D, Ainsworth K, Ayeni OR, Simunovic N, Peterson D. Juvenile osteochondritis dissecans of the knee: does magnetic resonance imaging instability correlate with the need for surgical intervention? Orthop J Sports Med. 2017;5:2325967117738516. [PubMed: 29164166]
42. Bolan PJ, Arentsen L, Sueblinvong T, et al. Water-fat MRI for assessing changes in bone marrow composition due to radiation and chemotherapy in gynecologic cancer patients. J Magn Reson Imaging. 2013;38:1578–1584. [PubMed: 23450703]

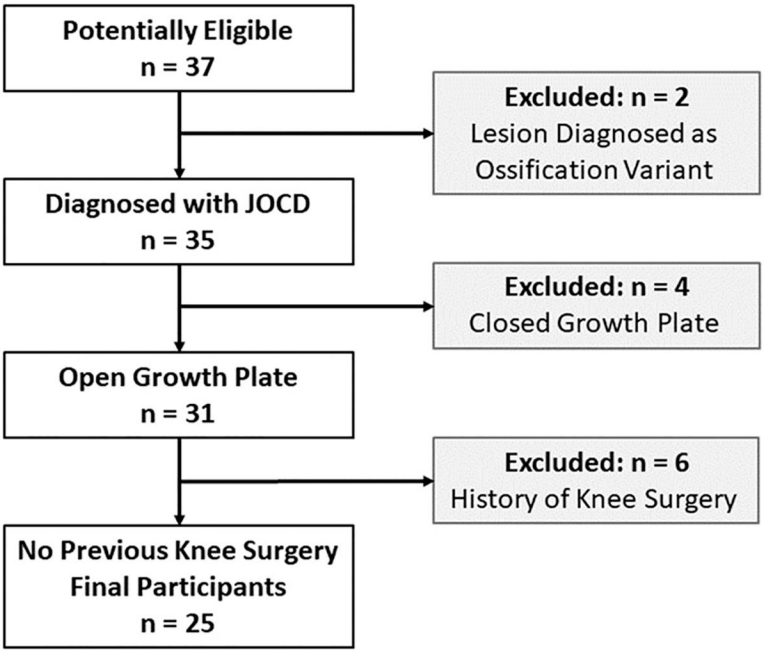

FIGURE 1.
Flowchart of study population

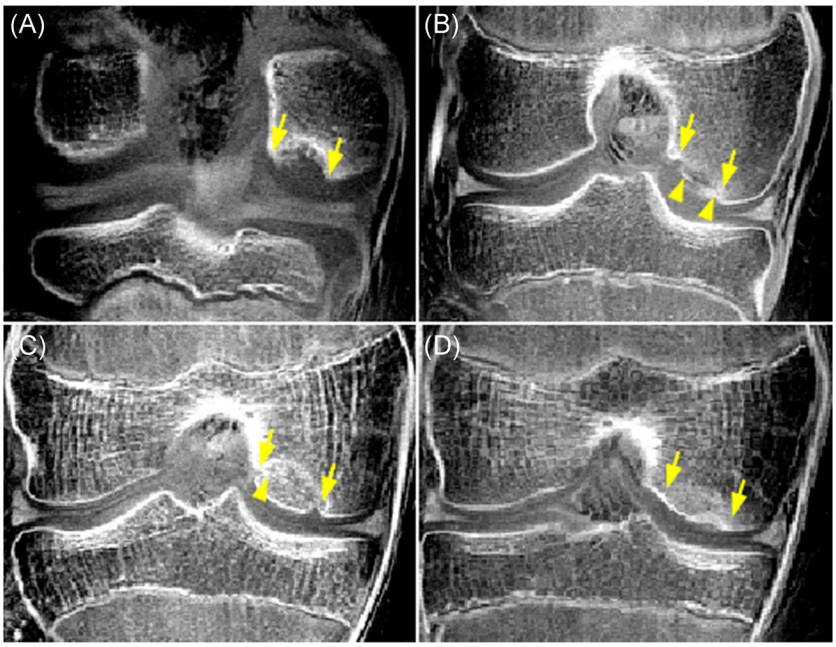

FIGURE 2.

A qualitative depiction of osseous tissues in JOCD lesions (between arrows) on the morphological, short echo time GRE images with CT-like contrast showing different stages of disease. (a) A 12-year-old boy with a stage I, cartilaginous-only lesion. (b) A 12-year-old girl with a stage II lesion showing ossification of the progeny rim (arrow heads). (c) A 14-year-old boy with a stage III, predominantly osseous progeny with a partial osseous bridging to parent bone (arrow head). (d) A 13-year-old girl with a stage IV, osseous, healed lesion. All lesions are located on the medial femoral condyle [Color figure can be viewed at wileyonlinelibrary.com]

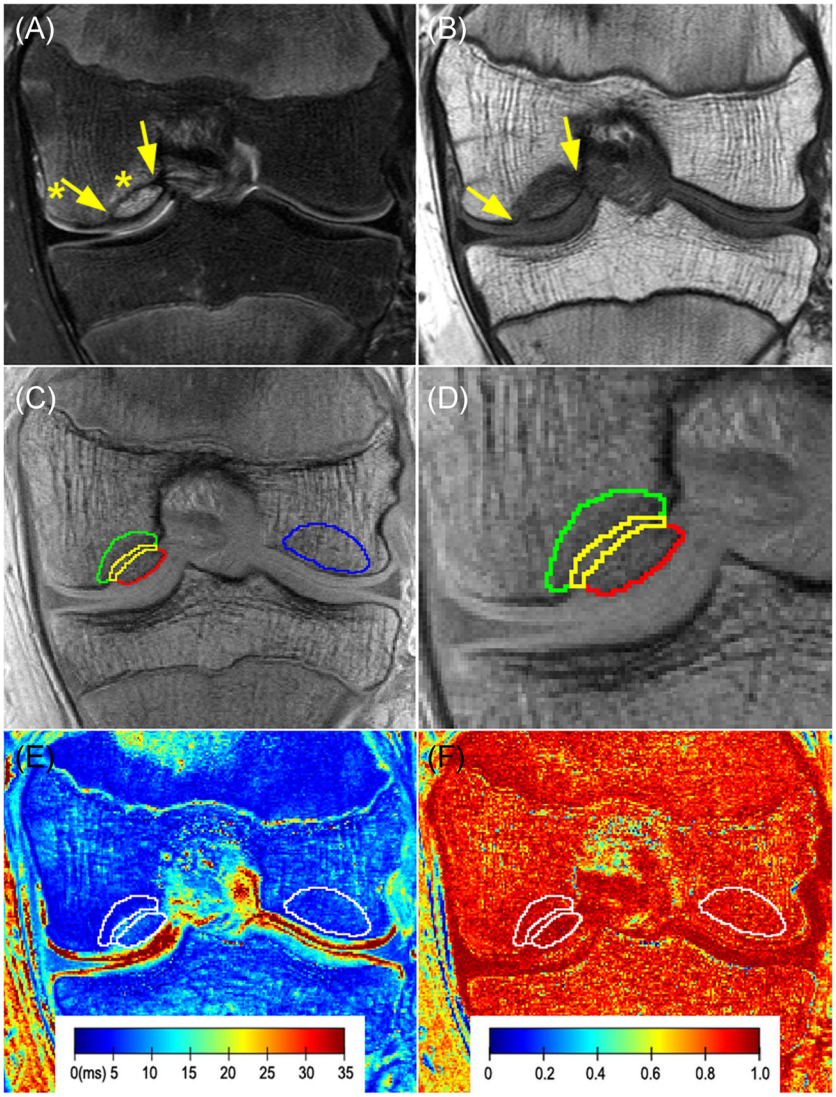

FIGURE 3.

An example of manual segmentations of the four evaluated regions on MR images of a 14-year-old boy with a stable, stage III JOCD lesion on the medial femoral condyle. (a) The T_2-weighted turbo spin echo image with fat suppression depicts the position of progeny lesion (between arrows) and interface as well as hyperintense edema in the parent bone (asterisks). (b) The T_1-weighted turbo spin echo image is showing a parent bone region with the replacement of normal fatty marrow (between arrows). (c) All four evaluated regions were selected on the first echo of the T_2*-weighted MR images. Three regions were part of the JOCD lesion complex: progeny lesion (red), interface (yellow) and parent bone (green). Additionally a control bone region (blue) served as a reference. (d) A higher magnification view of the JOCD lesion area showing progeny lesion, interface and parent bone detail. (e) Segmented regions (white contours) overlaid on the color-coded T_2* map; the color bar represents T_2* values in milliseconds. (f) The color-coded coefficient-of-determination (R^2) map with four segmented regions (white contours); the color bar represents R^2 values [Color figure can be viewed at wileyonlinelibrary.com]

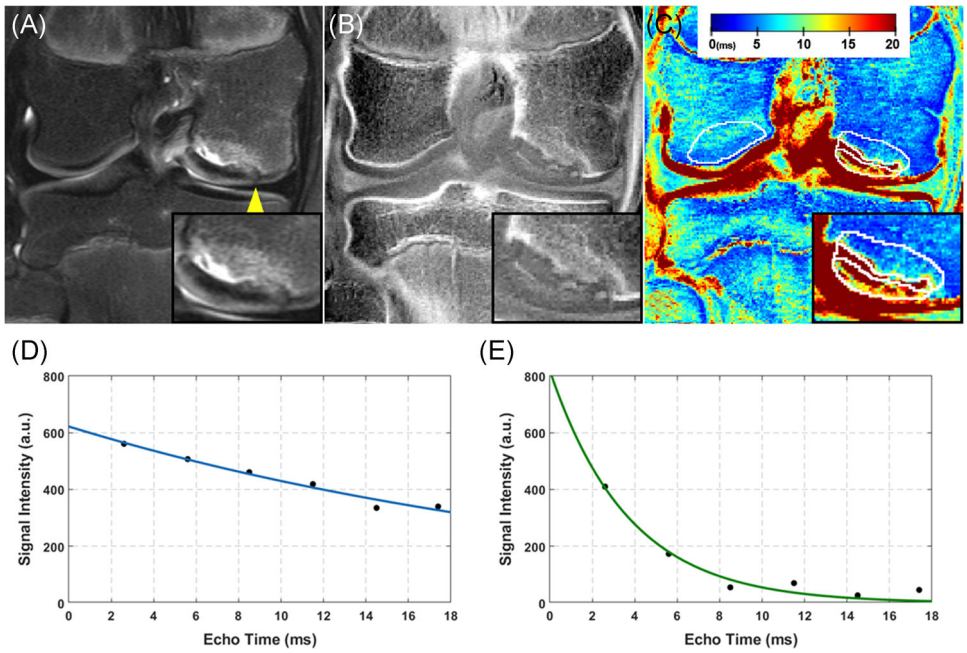

FIGURE 4.

A 12-year-old girl with a stage II unstable JOCD lesion on the medial femoral condyle. (a) The T_2-weighted turbo spin echo images with fat suppression depict the lesion location, a hyperintense area of edema in the parent bone, a fluid-like high signal rim in the interface and a break in the articular cartilage and the subchondral bone plate (arrowhead). (b) Short echo time gradient echo image with CT-like contrast showing a high signal of the progeny rim ossification and a low signal of cartilaginous areas in the progeny lesion and interface. (c) The corresponding color-coded T_2* map with four selected regions (white contours). Please note the parent bone with lower T_2* (blue areas) compared to the control bone region on the opposite condyle which may indicate a decrease in bone density in the parent bone. Additionally, T_2* map reflects the heterogeneous composition of progeny lesion region with high T_2* areas (red) being composed predominantly of cartilaginous tissue and low T_2* areas (green and blue) of osseous tissues. A higher magnification image of the JOCD lesion area is shown in the lower right corner of each image. The color bar represents T_2* values in milliseconds. (d) A plot showing a representative T_2* fit (blue line) of signal intensities (black points) as a function of echo time from a single pixel situated in the cartilaginous tissue in the progeny lesion shown in (a–c) (fitted T_2* = 27.1 ms; goodness of fit (R^2) = 0.963). (e) A representative T_2* fit of signal intensities as a function of echo time from a single pixel situated in the osseous area of progeny lesion shown in (a–c) (fitted T_2* = 3.7 ms; R^2 = 0.959). Please note the faster decay of signal intensities with echo time and therefore shorter T_2* when compared to the fit illustrated in (d) [Color figure can be viewed at wileyonlinelibrary.com]

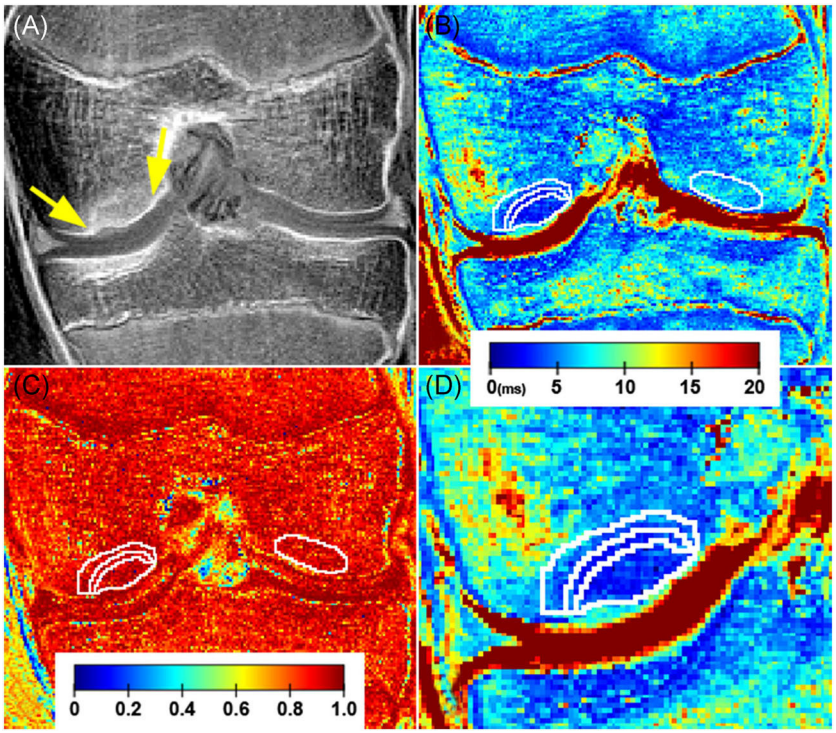

FIGURE 5.

A 13-year-old girl with a healed, stage IV JOCD lesion on the medial femoral condyle. (a) The first echo of the T_2*-weighted MR images with CT-like contrast showing osseous, healed lesion (between arrows). (b) The corresponding color-coded T_2* map with four selected regions in white contours: progeny lesion, interface, parent bone, and control bone on opposite condyle. Note the lower T_2* values in the progeny lesion than in the control bone region; the color bar represents T_2* values in milliseconds. (c) The color-coded coefficient-of-determination (R^2) map shows high agreement (close to 1) between the measured data and the exponential fit in all four evaluated regions (white contours); the color bar represents dimensionless R^2 values. (d) A zoomed-in depiction of the JOCD lesion area on T_2* map showing detail of progeny lesion, interface and parent bone; the color bar represents T_2* values in milliseconds [Color figure can be viewed at wileyonlinelibrary.com]

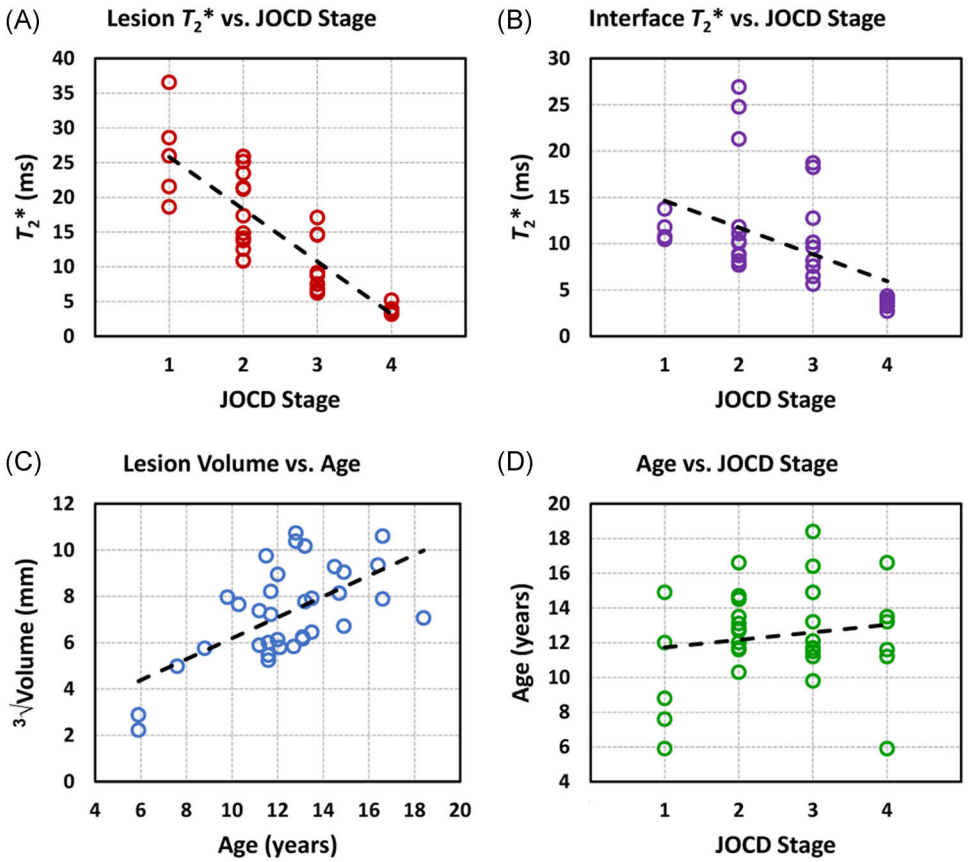

FIGURE 6.

Regression analysis plots. (a) A significant negative spearman rank correlation (ρ) was observed between the progeny lesion T_2* and the JOCD stage ($\rho = -0.871$; 95% confidence interval = −0.936, −0.732; $p < 0.001$). (b) A significant negative correlation was found between the interface T_2* and the JOCD stage ($\rho = -0.649$; 95% confidence interval = −0.834, −0.346; $p < 0.001$). (c) A significant positive correlation was observed between the progeny volume and the patient's age ($\rho = 0.534$; 95% confidence interval = 0.123, 0.753; $p = 0.001$). The high median T_2* values (>15 ms) in the interface at JOCD stages II and III can be explained by the presence of fluid in the interface which was detected with clinical, morphological MRI in eight unstable lesions. (d) The spearman rank correlation did not show any significant association between the patient's age and the JOCD stage ($\rho = 0.081$; 95% confidence interval = −0.331, 0.477; $p = 0.65$) [Color figure can be viewed at wileyonlinelibrary.com]

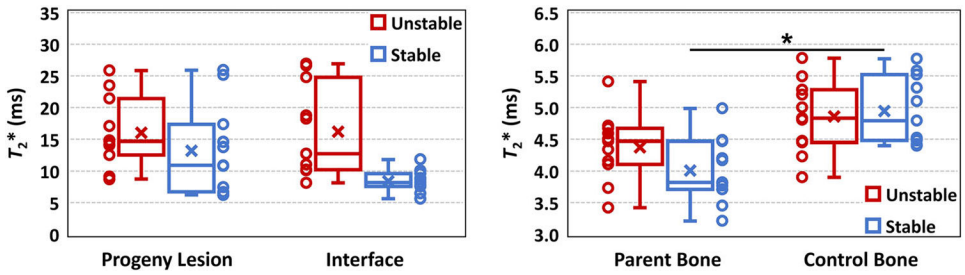

FIGURE 7.

Box plots of median T_2* from progeny lesion, interface, parent bone and control bone regions of eleven stable and eleven unstable JOCD lesions. Data points for each group and region are shown next to the corresponding box plot. The mixed effects regression models, with age, sex and progeny volume as covariates and adjustment for within-subject variability found significantly lower T_2* values in parent bone than in control bone in stable lesions (p = 0.009). The high variability of T2* values in the interface of unstable lesion, when compared to stable lesions, is likely due to the presence of fluid detected in 8 of 9 unstable lesions. In each box plot, the cross represents the mean T_2* value and the central horizontal line the median T_2* value of the evaluated region. The upper and lower whiskers extend to the maximum and minimum T_2* values in the region, respectively. The upper and lower borders of the box represent the third quartile (i.e., 75th percentile) and the first quartile (i.e., 25th percentile) of the T_2* data within the region, respectively [Color figure can be viewed at wileyonlinelibrary.com]

TABLE 1

Acquisition parameters of MRI sequences

Acquisition	**Axial FS**	**Sagittal**	**Sagittal FS**	**Coronal FS**	**Coronal**	**Coronal 2D**
Parameter	**T_2w TSE**	**PDw TSE**	**PDw TSE**	**T2w TSE**	**T_1w TSE**	**T_2* mapping**
Repetition time (ms)	3860	1810	2000	3860	786	1150
Echo time (ms)	36	37	32	47	9.3	2.6, 5.6, 8.5, 11.5, 14.5, 17.4
Flip angle (degrees)	150	150	150	150	150	60
Pixel BW (Hz/pix)	195	240	240	200	200	405
Field of view (mm^2)	130 × 130	110 × 110	110 × 110	110 × 110	110 × 110	150 × 150
Matrix size	256 × 233	256 × 218	256 × 218	320 × 224	320 × 224	352 × 352
Resolution[#] (mm^2)	0.51 × 0.51	0.43 × 0.43	0.43 × 0.43	0.34 × 0.34	0.34 × 0.34	0.43 × 0.43
Slice thickness (mm)	3.0	3.0	3.0	3.0	3.0	2.0
Number of slices	31	31	31	29	29	30–39
Echo train length	11	5	5	11	2	6
Number of averages	1	1	2	2	1	1
Freq.-encoding direction	A-P	A-P	A-P	F-H	F-H	R-L
Imaging time (min)	1:17	1:21	2:54	2:22	1:01	5:24–6:57

Abbreviations: A-P, anterior-posterior; BW, bandwidth; F-H, feet-head; Freq.-encod., frequency-encoding; FS, fat suppression; PDw, proton density-weighted; R-L, right-left; T_1w, T1-weighted; T_2w, T2-weighted; TSE, turbo spin echo.

[#]Reconstructed pixel size is reported.

TABLE 2

Demographic details of the study group and subgroups

Group	Number of knees (%)	Sex Male/female	Age (years) Median (IQR)	Laterality Right/left	Location MFC/LFC	Symptoms Yes/no	Lesion stability Stable/Unstab.
JOCD I	5 (10.6%)	3/2	8.8 (7.6–12.0)	3/2	2/3	4/1	5/0
JOCD II	13 (27.7%)	7/6	12.8 (12.0–13.5)	9/4	12/1	13/0	6/7
JOCD III	9 (19.1%)	8/1	12.1 (11.5–14.9)	1/8	8/1	9/0	5/4
JOCD IV	7 (14.9%)	3/4	11.6 (11.4–13.4)	2/5	4/3	3/4	7/0
Control	13 (27.7%)	9/4	11.7 (10.3–14.9)	8/5	N/A	0/13	N/A
Total	47 (100%)	30/17	12.1 (11.5–14.5)	23/24	26/8	29/18	23/11
Stable	11 (23.4%)	7/4	12.1 (11.7–13.1)	5/6	10/1	10/1	11/0
Unstable	11 (23.4%)	8/3	13.2 (12.3–16.5)	5/6	10/1	11/0	0/11

Abbreviations: IQR, interquartile range; JOCD, Juvenile Osteochondritis Dissecans, LFC, lateral femoral condyle; MFC, medial femoral condyle, Unstab., unstable.

TABLE 3

Comparison between different regions

		T_2* (ms)			R^2	Volume (mm^3)
Knee type	**Region**	**Median (IQR)**	***p* values**		**Median (IQR)**	**Median (IQR)**
JOCD Stage I *n* = 5	Progeny lesion	26.0 (21.6–28.6)	vs. IN, **<0.001**	vs. PB, **<0.001**	0.948 (0.943–0.956)	191 (124–230)
	Interface	10.7 (10.6–11.8)	vs. PB, =0.28	vs. CB, =0.62	0.958 (0.956–0.962)	120 (101–146)
	Parent bone	3.9 (3.6–3.9)	vs. CB, =0.98		0.935 (0.920–0.944)	377 (336–610)
	Control bone	4.2 (4.1–5.2)	vs. PL, =**0.008**		0.935 (0.934–0.939)	723 (537–828)
JOCD Stage II *n* = 13	Progeny lesion	17.4 (13.8–23.5)	vs. IN, =0.086	vs. PB, **<0.001**	0.953 (0.948–0.956)	539 (243–801)
	Interface	10.2 (8.7–11.8)	vs. PB, **<0.001**	vs. CB, **<0.001**	0.957 (0.943–0.962)	295 (120–346)
	Parent bone	4.3 (3.8–4.5)	vs. CB, =0.93		0.943 (0.935–0.950)	938 (525–1437)
	Control bone	4.8 (4.5–5.2)	vs. PL, **<0.001**		0.942 (0.937–0.944)	2177 (942–2306)
JOCD Stage III *n* = 9	Progeny lesion	8.7 (6.7–14.6)	vs. IN, =0.73	vs. PB, =**0.001**	0.951 (0.941–0.959)	470 (376–739)
	Interface	9.6 (7.6–12.7)	vs. PB, =**0.006**	vs. CB, =0.06	0.953 (0.945–0.964)	247 (155–323)
	Parent bone	4.2 (3.8–4.5)	vs. CB, =0.99		0.939 (0.919–0.947)	791 (769–1015)
	Control bone	5.1 (4.5–5.5)	vs. PL, =**0.025**		0.934 (0.925–0.947)	1454 (1127–1910)
JOCD Stage IV *n* = 7	Progeny lesion	3.5 (3.4–3.9)	vs. IN, =0.84	vs. PB, =0.45	0.936 (0.927–0.939)	216 (174–494)
	Interface	3.6 (3.3–3.8)	vs. PB, =0.34	vs. CB, =0.11	0.927 (0.917–0.937)	64 (54–120)
	Parent bone	4.0 (3.9–4.3)	vs. CB, =0.17		0.933 (0.925–0.942)	424 (240–595)
	Control bone	4.9 (4.4–5.3)	vs. PL, =**0.028**		0.927 (0.925–0.945)	609 (458–1081)
Control *n* = 13	Control bone	5.0 (4.6–5.4)	vs. CB in JOCD, =0.06		0.938 (0.922–0.940)	1545 (870–2024)

Abbreviations: CB, control bone; IN, interface; IQR, interquartile range; JOCD, Juvenile Osteochondritis Dissecans; PB, parent bone; PL, progeny lesion; R^2, coefficient of determination.

TABLE 4

Comparisons between different JOCD stages

Lesion stage	Progeny T_2*	Interface T_2*	Parent bone T_2*	Control bone T_2*	Progeny volume
I vs. II	0.053	0.95	0.66	0.47	0.17
I vs. III	**<0.001**	0.75	0.70	0.12	0.40
I vs. IV	**<0.001**	**0.003**	0.49	0.43	0.66
II vs. III	**0.011**	0.83	0.99	0.67	0.94
II vs. IV	**<0.001**	**0.020**	0.99	0.99	0.72
III vs. IV	0.35	**0.046**	0.98	0.73	0.97

Note: Data are *p* values. Bold numbers indicate statistically significant differences.

TABLE 5

Spearman rank correlation analyses

	Region			
	Progeny Lesion	**Interface**	**Parent Bone**	**Control Bone**
T_2* values vs. JOCD stage				
Spearman	**−0.871**	**−0.649**	0.107	0.210
p value	**<0.001**	**<0.001**	0.55	0.23
95% CI	**−0.936/−0.732**	**−0.834/−0.346**	−0.252/0.427	−0.161/0.576
T_2* values vs. age				
Spearman	−0.111	0.010	−0.040	−0.177
p value	0.53	0.58	0.83	0.32
95% CI	−0.441/0.260	−0.267/0.436	−0.369/0.308	−0.525/0.197
Region volume vs. JOCD stage				
Spearman	0.109	−0.231	−0.105	
p value	0.54	0.19	0.55	N/A
95% CI	−0.297/0.475	−0.566/0.134	−0.475/0.279	
Region volume vs. age				
Spearman	**0.534**	**0.477**	**0.415**	
p value	**0.001**	**0.004**	**0.014**	N/A
95% CI	**0.123/0.753**	**0.165/0.704**	**0.106/0.681**	

Note: Bold numbers indicate statistically significant correlations.

Abbreviations: CI, confidence interval; JOCD, Juvenile Osteochondritis Dissecans.

TABLE 6

Comparison between stable and unstable JOCD lesions

	T_2* (ms) Median (IQR)				Volume (mm^3) Median (IQR)
Lesion type	**Progeny lesion**	**Interface**	**Parent bone**	**Control bone**	**Progeny lesion**
Stable	10.8 (6.7–17.2)	5.6 (5.5–8.9)	3.7 (3.3–3.8)	5.2 (4.6–5.3)	199 (184–376)
Unstable	14.7 (13.3–19.2)	12.7 (10.2–21.7)	4.5 (4.1–4.6)	4.8 (4.5–5.2)	801 (458–1022)
p value	0.29	0.27	0.74	0.98	**0.002**

Note: Bold number indicate statistically significant correlations.

Abbreviation: IQR, interquartile range.